PCCP

# Evidence for Near-Superionic Conductivity in the Li3BS3 Electrolyte and Insights on the Lithium Orthothioborate Transport Mechanisms



| | |
|---|---|
| Journal: | *Physical Chemistry Chemical Physics* |
| Manuscript ID | CP-ART-09-2024-003771.R2 |
| Article Type: | Paper |
| Date Submitted by the Author: | 11-Jan-2025 |
| Complete List of Authors: | Riasati, Aarya; California Institute of Technology, Chemistry<br>Das, Tridip; California Institute of Technology, Materials and Process Simulation Center<br>Goddard III, William; California Institute of Technology, |
| | |

# Evidence for Near-Superionic Conductivity in the $Li_3BS_3$ Electrolyte and Insights on the Lithium Orthothioborate Transport Mechanisms

Aarya D. Riasati, Tridip Das, William A. Goddard III*

Materials and Process Simulation Center, California Institute of Technology, Pasadena, CA, 91125, USA

* Corresponding author, wag@caltech.edu

ORCID: WAG:0000-0003-0097-5716

AR: 0000-0003-0974-5968

TD: 0000-0002-3320-2157

## Abstract

In developing battery technology toward Li anode systems rather than Li ion, it has become necessary to discover superior ionic conductors for solid-state electrolyte batteries. $Li_3BS_3$ is among these candidate superior ionic conductors.[1] We report here Molecular Dynamics (MD) simulations to predict the diffusivity, conductivity, and activation energy for $Li^+$ transport in Lithium Orthothioborate ($Li_3BS_3$) as a function of temperatures using the Universal Force Field (UFF) force field retrained with Quantum Mechanics (QM). This leads to an ionic conductivity of ~2.1 mS/cm with an activation energy of ~+0.19 eV (+18.2 kJ) at 300 K and 1 atm, based on 20 ns of MD.[2] These results are in good agreement with experiments (0.1 to 10 mS/cm) on -$PS_4$ based argyrodite electrolytes with similar activation energies (0.15 to 0.5 eV). Our calculations indicate that $Li_3BS_3$ is a superior ionic conductor, with potential as a future electrolyte for solid-state Li anode batteries.

## Introduction

Lithium-ion batteries play an important role in energy and climate sustainability to enable new strategies for clean energy production and storage. Li metal anodes have the potential to dramatically reduce the power per weight ratio (by a factor of >4), which would be highly desirable to meet electric vehicle goals of 2030. In particular, superionic electrolytic solid-state materials, such as $Li_3BS_3$, would by desirable for enhanced battery performance. $Li_3BS_3$ and associated derivatives demonstrate superionic $Li^+$ conductivity, and as solid-state electrolytics they are safer for practical applications as compared to traditional liquid-based electrolytes.[3]

Lithium Orthothioborate, $Li_3BS_3$ and associated $Li_3MX_6$ and $Li_3MX_3$ derivatives have received attention due to their high temperature conductivity and stability.[4, 5] In particular, cationic stability due to increased anionic packing during synthesis results in novel migration pathways as a result of its disordered trigonal lattice parameters. This results in low thermal activation energies. This, alongside the high temperature conductivity and oxidative stability of the $Li_3MX_3$ crystal makes it particularly appealing as an ionic conductor. In this paper, we predict the conductivity properties of Lithium Orthothioborate using Molecular Dynamics (MD) with a force field trained using QM to calculate activation barriers for migration of $Li^+$ (and the other) ions as a function of temperature. To predict accurate diffusivities, we use the Einstein relation, which requires MD simulations for ~10 nanoseconds to achieve the Fickian regime of random walk diffusion in which log (RMSD) is proportional to Log (time), where RMSD is root mean squared displacement. Such nanosecond MD are practical for FF but not for quantum mechanical (QM) MD such as AIMD, which is

practical for systems with <300 atoms for timescales <100ps. Consequently, we use a QM trained FF to study diffusivity and conductivity.

**Computational Methods**

To assess the feasibility of $Li_3BS_3$ for ionic conductivity, we started with Periodic Density Functional Theory (DFT) calculations using the Vienna Ab-Initio Simulation Package (VASP) with the PBE-D3[6] DFT functional.[7] First, we minimized the structure to serve as the starting point for the MD.

Then, to calculate diffusion on a large unit cell for 20 ns, we adjusted the parameters of the Universal Force Field (UFF)[8] to match B-S bond distances from DFT, and we adjusted the UFF nonbond and electrostatic parameters match the experimental bond lengths and density at room temperature (293 K) to within 5% accuracy. We also induced a 2% vacancy to mimic cell imperfections and defects commonly seen in experimental conditions.

To setup the initial conditions for MD simulations, the following steps were taken:

1. Scaled charges were assigned using the DDEC6[9] method to each individual atom in the minimized structure obtained from initial QM VASP calculations. These charges were used as point charges throughout all remaining steps.[10]

2. Constant volume temperature thermostat (NVT) simulations at 10K for 10ps were used to generate initial velocities.

3. Heating of the periodic box from 10K to 300K over 100ps using NVT conditions.

4. Constant pressure and temperature (NPT) simulations for 20 ns at 293 K for 20 ns, followed by NVT-MD simulations at ~ 1 atm pressure at various temperatures between 200K and 600K. A Berendsen thermostat damping time of 0.1 ps was used to describe temperature fluctuations in the system.

We performed 20 ns NVT-MD simulations to reach Fickian behavior [log (MSD) proportional to log (time)] to extract diffusion coefficients for ionic conduction of Li+ and other ions . The diffusion was predicted as a function of temperature to obtain activation energies. We report the results of anion and cation diffusion in $Li_3BS_3$ over the range from 200K to 600K, where we observed superionic conductivity for $Li_3BS_3$, as expected.

Following completion of MD at each temperature, ion diffusion coefficients (D) were derived from a mean square displacement (MSD) using the Nernst-Einstein diffusion equation.

$$\mathrm{MSD}(t) \equiv \langle (r(t) - r(t_0))^2 \rangle = 6Dt$$

where MSD for time t is the average MSD for that time increment averaged over the whole 20 ns trajectory. To obtain D we plot log MSD vs Log t to find the point at which the slope is unity (Fick condition). The intercept then gives 6D.

Based on the diffusivity constant, D, from MD, we used the Nernst-Einstein equation (2) to predict the conductivity σ.

$$\sigma = \frac{DNq^2}{\mathrm{RT}} \qquad (2)$$

Here, N is the number of charge carriers per unit cell, q is the charge of the ion, , R is the gas constant, and T is temperature. In these calculations we assume q = +1 for the $Li^+$ ion.

The activation energy ($E_a$) is computed following the modified Arrhenius equation for conductivity (3). For solid-state diffusion, the pre-factor is temperature-dependent due to variations in jump frequency and jump distance The standard Arrhenius equation is more suitable for the kinetic theory of gasses.[11] Therefore, we must use the modified Arrhenius equation:

$$\sigma T = \sigma_o exp\left(\frac{-E_a}{k_b T}\right) \quad (3)$$

**Results and Discussion**

| Temperature | Diffusivity ($cm^2/s$) | Conductivity (S/cm) |
|---|---|---|
| 200K | 3.62E-09 | 7.60E-04 |
| 300K | 1.60E-08 | 2.21E-03 |
| 400K | 3.41E-08 | 3.47E-03 |
| 425K | 1.14E-07 | 1.12E-02 |
| 450K | 9.87E-08 | 9.64E-03 |
| 475K | 1.45E-07 | 1.29E-02 |
| 500K | 6.74E-06 | 5.63E-01 |
| 600K | 2.89E-05 | 1.95E-00 |

Table 1. Diffusivity and conductivity values for $Li_3BS_3$ as a function of temperature. Temperatures from 200K to 600K.

We calculate the ion migration number to be 0.94. Previous computational analyses predict the electrochemical stability window to be +0.45 V.[12] As shown in Table 1 there is a sharp increase in conductivity between 400K to 500K, with significantly increased disorder in B and S at 500K. As a result, secondary effects from increased lattice disorder in the $Li_3BS_3$ supercell dramatically increase $Li^+$ diffusion rate and conductivity above 400K. Increases in secondary diffusion in B and S would allow for increased diffusion for Li, as vacancy sites present in the lattice as a result of B and S movement would increase Li hopping. This would be similar to AgI, where a structural phase transition from the β-phase hexagonal close-packed (HCP) structure to the t α-phase body-centered cub (BCC) structure increases conductivity by a factor of 100.[13] In the $Li_3PS_4$ electrolyte, there is also a structural phase transition from the β to α-phase due to increased disorder as temperature increases. This phase transition occurs from 573 to 758K.

Although we have not characterized the nature of the phase transition in $Li_3BS_3$, the behavior is similar to that found in $Li_3PS_4$, in which a first-order transition occurs.[14]

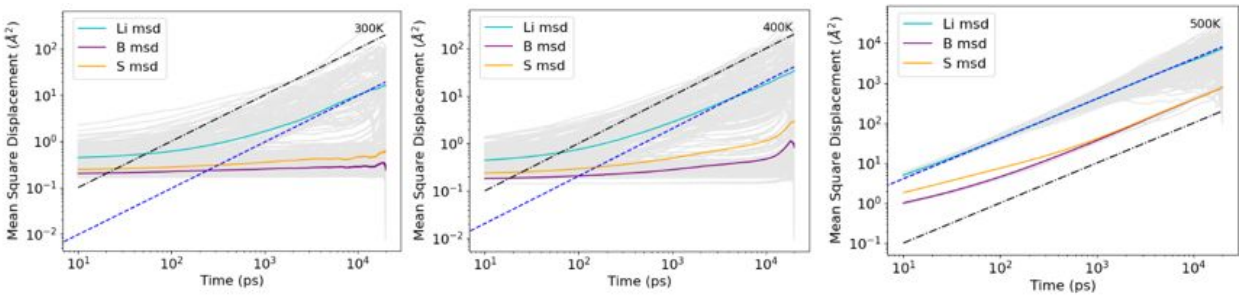


Figure 1. Mean Square Displacement versus time at 300K (left), 400K(middle) and 500K (right). The grey lines show each Li while the average over all Li is in turquoise. The plots for other T are in the SI. We see a big change in B and S diffusion between 400 and 500K. S is depicted in yellow, Li in turquoise, and B in purple.

Fig. 2 shows that the predicted conductivity increases dramatically between 400K and 500K. We find that this elevated diffusion arises from increase vacancies present in the crystal lattice above 400K. This, alongside elevated thermal energy and entropy in $Li^+$ as a result of increased temperature, increases overall conductivity values drastically, by 1.6E+04 % at 425 K, with drastic changes also occurring from 450 to 475K.

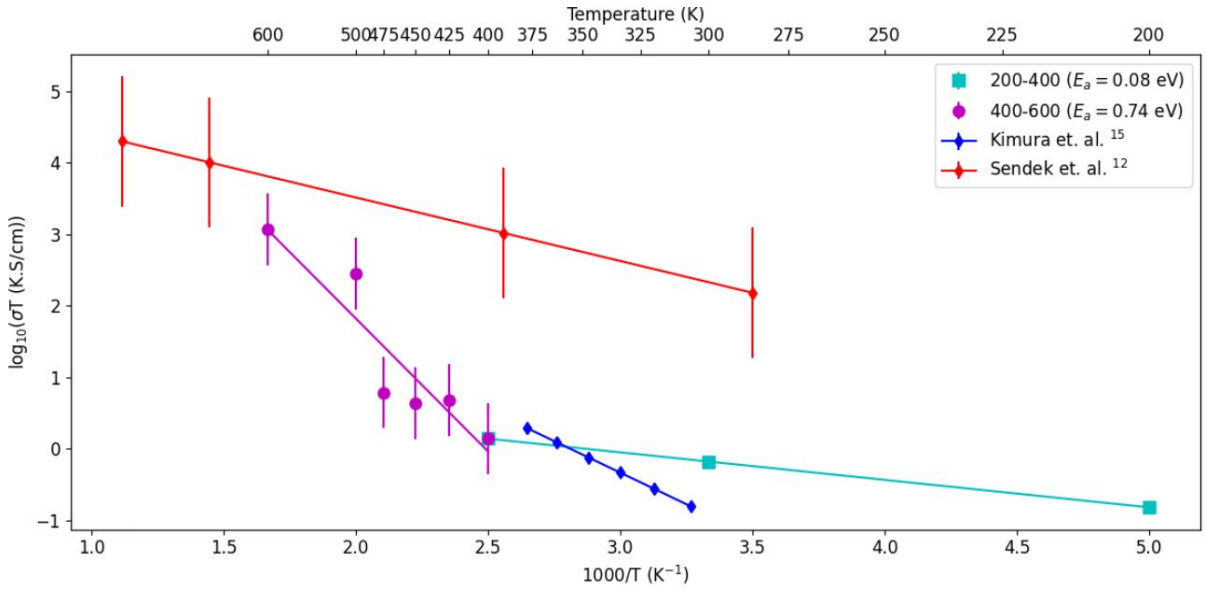


Figure 2. Log-plot of ion conductivity times temperature (T) for Li3BS3 from 200-400K and 400-600K. Unit cell structures were optimized using NPT. Other studies on $Li_3BS_3$ and similar derivatives are also shown.

Previous experimental analyses of $Li_3BS_3$ glass, formed by melt-quenching the $Li_3BS_3$ crystal by heating the system to 1000K then cooling to 300K to form the glass, found ionic conductivities on the order of magnitude of 0.336 mS/cm at 298K with an activation barrier of 0.33 eV over the range of 200 to 600K.[15] Our simulations find activation energy of +0.08 eV from 200-400K, but an activation energy is +0.74 eV from the temperature range of 400-600K. Deviation of our MD-predicted diffusivity and conductivity values from experimental values may arise from inhomogeneities in the experimental samples and defects present in a $Li_3BS_3$ glass.[16] Here, we use the term "defect" to include impurities, phase separation, clustering, coordination defects, substitutional defects, vacancies, etc.

Ab-Initio Molecular Dynamics using DFT of the plane-wave (PAW) implementation of the Vienna Ab-Initio simulation package (VASP) found ionic conductivities ranging from $10^{-6}$ to $10^{-3}$ mS/cm at 300K with barriers ranging from 0.08 eV to 0.25 eV, depending on the direction of $Li^+$ diffusion in the lattice. Movement along the c-direction led to an activation barrier of 0.08 eV, whereas movement along the path connecting the (a,c) layers found activation barriers of 0.25 eV. However, these time scales of <100 ps were too short for reliable conductivities.[17]

These results indicate potential application of $Li_3BS_3$ and its derivatives as superionic electrolytes.

## Conclusion

$Li_3BS_3$ is predicted to display superionic conductivity of 2.1 mS/cm at 300K. This, and its low activation energy for $Li^+$ migration through the lattice (~ +0.19 eV), make $Li_3BS_3$ a good candidate electrolyte for the development of advanced solid-state batteries.

In addition, doping of $Li_3BS_3$ holds promise to further enhance its conductivity.[17] Thus introducing 1-12% Si or Ge based dopants into the system may increasing its conductivity past $10^{-3}$ S/cm, making $Li_3BS_3$ quite promising for battery application developments.

## Acknowledgements

AR conceived the project and carried out the calculations with input from TD. AR wrote the paper with contributions from WAG and TD.

This work was supported by the Hong Kong Quantum AI Lab, AIR@InnoHK of the Hong Kong Government and by the US National Science Foundation (CBET-2311117)

## Conflict of Interest

The authors declare no conflict of interest.

References

1. Vinatier P, Gravereau P, Ménétrier M, Trut L, Levasseur A. Li3BS3. *Acta Crystallogr C.* 1994;50:1180–3.
2. Thompson AP, Aktulga HM, Berger R, Bolintineanu DS, Brown WM, Crozier PS, et al. LAMMPS - a flexible simulation tool for particle-based materials modeling at the

atomic, meso, and continuum scales. *Comput Phys Commun.* 2022;271:108171. doi:10.1016/j.cpc.2021.108171.
3. Das T, Yang MY, Merinov BV, Goddard WA. Atomistic Simulations of Battery Materials and Processes. In: *Hanaor DAH*, editor. Computational Design of Battery Materials. Cham: Springer International Publishing; 2024. p. 13–76. doi:10.1007/978-3-031-47303-6_2.
4. Schlem R, Banik A, Ohno S, Suard E, Zeier WG. Insights into the Lithium Sub-structure of Superionic Conductors Li3YCl6 and Li3YBr6. *Chem Mater.* 2021;33(1):327–37. doi:10.1021/acs.chemmater.0c04352.
5. Yang S, Kim SY, Chen G. Halide Superionic Conductors for All-Solid-State Batteries: Effects of Synthesis and Composition on Lithium-Ion Conductivity. *ACS Energy Lett.* 2024;0:2212–21. doi:10.1021/acsenergylett.4c00317.
6. Perdew JP, Burke K, Ernzerhof M. Generalized Gradient Approximation Made Simple. *Phys Rev Lett.* 1996;77(18):3865–8. doi:10.1103/PhysRevLett.77.3865.
7. Kresse G, Hafner J. Ab initio molecular dynamics for liquid metals. *Phys Rev B.* 1993;47(1):558–61. doi:10.1103/PhysRevB.47.558.
8. Rappe AK, Casewit CJ, Colwell KS, Goddard WA III, Skiff WM. UFF, a Full Periodic Table Force Field for Molecular Mechanics and Molecular Dynamics Simulations. *J Am Chem Soc.* 1992;114(25):10024–35. doi:10.1021/ja00051a040.
9. Manz TA, Limas NG. Introducing DDEC6 atomic population analysis: part 1. Charge partitioning theory and methodology. *RSC Adv.* 2016;6(53):47771–801. doi:10.1039/C6RA04656H.
10. Das T, Merinov BV, Yang MY, Goddard WA III. Structural, dynamic, and diffusion properties of a Li6(PS4)SCl superionic conductor from molecular dynamics simulations; prediction of a dramatically improved conductor. *J Mater Chem A.* 2022;10(30):16319–27. doi:10.1039/D2TA02715A.
11. Feng X, Chien P-H, Wang Y, Patel S, Wang P, Liu H, et al. Enhanced ion conduction by enforcing structural disorder in Li-deficient argyrodites Li6−xPS5−xCl1+x. *Energy Storage Mater.* 2020;30:67–73. doi:10.1016/j.ensm.2020.04.042.
12. Sendek AD, Antoniuk ER, Cubuk ED, Ransom B, Francisco BE, Buettner-Garrett J, et al. Combining Superionic Conduction and Favorable Decomposition Products in the Crystalline Lithium–Boron–Sulfur System: A New Mechanism for Stabilizing Solid Li-Ion Electrolytes. *ACS Appl Mater Interfaces.* 2020;12(34):37957–66. doi:10.1021/acsami.9b19091.
13. Lee J-S, Adams S, Maier J. Transport and phase transition characteristics in AgI composite electrolytes: Evidence for a highly conducting 7-layer AgI polytype. *J Electrochem Soc.* 2000;147(6):2407-18. doi:10.1149/1.1393515.
14. Homma K, Yonemura M, Kobayashi T, Nagao M, Hirayama M, Kanno R. Crystal structure and phase transitions of the lithium ionic conductor Li3PS4. *Solid State Ion.* 2011;182(1):53–8. doi:10.1016/j.ssi.2010.10.001.
15. Kimura T, Inoue A, Nagao K, Inaoka T, Kowada H, Sakuda A, et al. Characteristics of a Li3BS3 Thioborate Glass Electrolyte Obtained via a Mechanochemical Process. *ACS Appl Energy Mater.* 2022;5(2):1421–6. doi:10.1021/acsaem.1c02452.
16. Fertig D, Stephan S. Influence of dispersive long-range interactions on transport and excess properties of simple mixtures. *Mol Phys.* 2023;121(19–20). doi:10.1080/00268976.2022.2162993.

17. Bianchini F, Fjellvåg H, Vajeeston P. A first-principles investigation of the Li diffusion mechanism in the super-ionic conductor lithium orthothioborate Li3BS3 structure. *Mater Lett.* 2018;219:186–9. doi:10.1016/j.matlet.2018.02.083.
18. Laskowski FA, McHaffie DB, See KA. Identification of Potential Solid-State Li-Ion Conductors with Semi-Supervised Learning. *ChemRxiv.* 2022. doi:10.26434/chemrxiv-2022-2m3qb. Preprint.

The data supporting this article have been included as part of the Supplementary Information.